

# Nonlinear viscoelastic isolation for seismic vibration mitigation

N. Menga,<sup>1,2,\*</sup> F. Bottiglione,<sup>1</sup> and G. Carbone<sup>1,2,3</sup>

<sup>1</sup>*Department of Mechanics, Mathematics and Management,  
Politecnico of Bari, V.le Japigia, 182, 70126, Bari, Italy*

<sup>2</sup>*Imperial College London, Department of Mechanical Engineering,  
Exhibition Road, London SW7 2AZ*

<sup>3</sup>*CNR - Institute for Photonics and Nanotechnologies U.O.S. Bari,  
Physics Department "M. Merlin", via Amendola 173, 70126 Bari, Italy*

## Abstract

The aim of this paper is to assess the effectiveness of nonlinear viscoelastic damping in controlling base-excited vibrations. Specifically, the focus is on investigating the robustness of the nonlinear base isolation performance in controlling the system response due to a wide set of possible excitation spectra. The dynamic model is derived to study a simple structure whose base isolation is provided via a Rubber-Layer Roller Bearing (RLRB) (rigid cylinders rolling on rigid plates with highly damping rubber coatings) equipped with a nonlinear cubic spring, thus presenting both nonlinear damping and stiffness. We found that, under periodic loading, due to the non-monotonic bell-shaped viscoelastic damping arising from the viscoelastic rolling contacts, different dynamic regimes occur mostly depending on whether the damping peak is overcome or not. Interestingly, in the former case, poorly damped self-excited vibrations may be triggered by the steep damping decrease.

Moreover, in order to investigate the robustness of the isolation performance, we consider a set of real seismic excitations, showing that tuned nonlinear RLRB provide loads isolation in a wider range of excitation spectra, compared to generic linear isolators. This is peculiarly suited for applications (such as seismic and failure engineering) in which the specific excitation spectrum is unknown a priori, and blind design on statistical data has to be employed.

Keywords: RLRB, viscoelastic damping, nonlinear friction, base isolation, robustness

---

\*Electronic address: [Corresponding author. ]Email: nicola.menga@poliba.it, phone number: +39 080 5962746

## I. INTRODUCTION

Controlling structural vibration is a long-standing problem and a key design requirement in several applications, as witnessed by the huge effort made in the last decades in developing innovative devices, and associated modelling methodology, specifically suited for this purpose. Moreover, the range of engineering branches facing this problem is definitely wide as all systems involving moving parts lead to vibrations.

It is, for instance, the case of wind turbine whose vibration generates both from internal (e.g. rotordynamics balancing, powertrain transmission) and external (wind action, marine waves) sources. In this case, several controlling techniques have been proposed [1], mostly based on passive mass-dampers [2] in the form of both ball vibration absorbers [3, 4] and tuned liquid column [5, 6]. Active techniques have also been tested using, for instance, synthetic jets to reduce aerodynamically induced blade vibrations [7]. Similarly, also the isolation of large industrial machineries is a challenging issue [9]. In this case, regardless of the vibration source, specific solutions have been developed to fulfill NVH requirements, such as adopting hybrid spring-actuator systems [8], semi-active pneumatic suspension with tunable inflating pressure [10], and active actuators with specific control strategies [11].

Of course, active systems are usually able to provide higher performance in vibration control; however, these are often costly while offering relatively low reliability due to their intrinsic higher complexity. Furthermore, their applicability to large scale problems is usually limited by the availability of appropriate actuators. Passive systems are therefore preferred when dealing with sufficiently large systems. It is the case, for instance, of ensuring high reliability to primary building such as hospitals, schools, museums and power plants [12], as well as structural control in bridges, with strong social, political, and economic implications. In this view, nonlinear passive isolation techniques are probably the most promising, as the nonlinearity can lead to better isolation performance in a much wider input spectrum. For these reasons, several possible source of nonlinearity have been explored in the last few decades. Indeed, the piecewise nonlinear behavior arising in both frictional dissipators [13] and bi-component sacrificial connections [14] has been exploited aiming at controlling the inter-story drift caused by earthquake excitations in high-rise structures, showing good results in terms of reduction of peak loads. On the contrary, for low-rise heavy buildings base isolation is usually preferred. Among them, several rolling isolation systems have been proposed (see Ref. [15]), most of which, by employing non-planar rolling paths, are able to produce a high-order nonlinear re-centering force [16, 17].

Similarly, vibration mitigation also by means of nonlinear damping has been increasingly explored [18, 19], mostly because of their ability to overcome typical limitations of linear dampers [20] (e.g. large reaction forces at high velocity, narrow effective frequency bandwidth) when dealing, for instance, with wind or earthquake nonstationary stochastic excitations. Among the others, these include nonlinear energy sink (NESs), particle impact dampers (PIDs), and nonlinear viscous dampers (NVDs), each of which presents his own specific advantage with respect to linear systems, as indeed reviewed in Ref. [21]. Although, NESs and PIDs have been successfully applied in controlling civil structures response to seismic motion [22–26], their primary fields of application range from aerospace [27–30] to machinery [31–33, 35] and lifeline [34, 36–39] engineering. On the contrary, NVDs have been increasingly utilized in civil engineering in the recent years [40–42]. This is because their damping force only depends on velocity, thus it results out-of-phase with the structural deformation and eventually leads to an overall reduction of loads and displacements on the

system [43]. Furthermore, the damping nonlinearity may lead to wider hysteretic cycles, associated to larger energy dissipation [44, 45].

Most of NVDs rely on damping force curves in the form  $F_d = C \text{sgn}(\dot{x}) |\dot{x}|^\alpha$  which, regardless of the  $\alpha$  exponent value, leads to a monotonic response with the deformation velocity  $\dot{x}$ . However, NVDs based on viscoelastic materials result in both nonlinear and non-monotonic damping behavior [45], thus leading to a limit on the maximum damping force, with possible benefits on the overall load transmissibility. NVDs devices for base isolation of civil structures from earthquake shocks have been already proposed so far in the form of Rubber-Layer Roller Bearings (RLRB), where both metal balls [46–50] and rollers [51–53] are interposed between plates coated with viscoelastic rubber layers. Although very effective in dissipating horizontal seismic components, these systems may suffer uplifts due to severe vertical accelerations in near-fault earthquake [54], which can only be partially remotely accommodated into the deformable rubber coatings. Nonetheless, the investigation of the base isolation performance of an RLRB viscoelastic damper with linear stiffness has recently shown promising results [55], as significantly lower stresses can be achieved on a simple base-isolated structure, in comparison with linear base isolation, as a result of the optimization of the nonlinear damping on a specific seismic excitation. However, since real processes are always stochastic at some degree (e.g. earthquakes, machinery failure, wind) [56], excitation spectra can be unknown and blind procedures have to be employed to design specific isolation systems, which are therefore required to present the broadest possible effective frequency bandwidth. For these reasons, here we focus on a fully nonlinear base isolation scheme relying on nonlinear viscoelastic damping (through an RLRB) associated with nonlinear stiffness (via a cubic spring). The aim is to assess whether full nonlinearity can effectively increase the isolation performance robustness over a set of excitations with different spectra, such as different seismic shocks. To pursue this target, building on an accurate previously developed [59, 61, 62, 64] Boundary Element Method (BEM) description of the contact interaction between the rigid rollers and the viscoelastic thin coating, we firstly investigate the nonlinear dynamics of such a system under periodic excitation, also investigating self-excited vibration induced by the steep decreasing portion of the bell-shaped viscoelastic damping force; then, assessing the performance robustness, we globally optimize both the nonlinear RLRB and the generic linear isolator over a set of five real seismic shocks, eventually comparing the performance of the two systems for each single shock in the globally optimized conditions.

## II. FORMULATION

A functional scheme of the system under investigation is shown in Figure 1a where a RLRB device of mass  $m_1$  equipped with a nonlinear spring is interposed between the ground and a very simple superstructure represented by an heavy inertial mass  $m_2$  supported by an elastic beam with bending stiffness  $k_s$ . Since in this study we aim at investigating the fundamental dynamic behavior of the system, we restrict our study to the case of purely horizontal excitations.

As shown in the lumped scheme reported in Figure 1b, two parallel nonlinear elements connect the superstructure to the ground: the RLRB nonlinear damper, and the nonlinear elastic element. Regarding the latter, in this study we focus on a cubic nonlinear spring, so that  $F_{el}(z) = \mu z^3$ , where  $z$  is the RLRB displacement, i.e. the relative displacements between the ground and the superstructure base.

Within the RLRB, a nonlinear damping force arises due to the rolling contact between

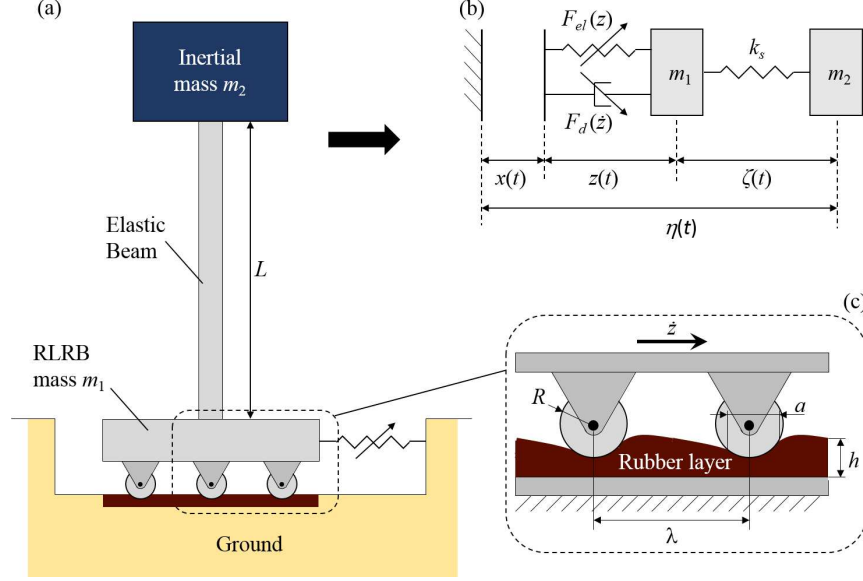


FIG. 1: A sketch of the two degree-of-freedom base-isolation scheme under investigation (a). The ground vibration  $x$  is filtered by means of the RLRB nonlinear damping force  $F_d$ , and the nonlinear elastic term  $F_{el}$ . The inertial mass  $m_2$  is supported by an elastic beam of linear stiffness  $k_s$ . On the top right (b): a lumped element scheme where  $z$  and  $\zeta$  are the relative displacement between the ground and the RLRB, and RLRB and inertial mass, respectively. On the bottom right (c): an RLRB close-up showing the rolling contact between the rigid rollers of radius  $R$  and the viscoelastic rubber layer of thickness  $h$ . Due to viscoelasticity, asymmetric contact occurs, thus leading to the nonlinear damping force  $F_d$ .

the rigid rollers and the viscoelastic coating, as already shown in Refs. [45, 55]. Specifically, the viscoelastic material response is represented by the viscoelastic complex modulus  $E(\omega)$ , which is a nonlinear function of the excitation frequency  $\omega$ . In the case of a single relaxation time  $\tau$  material, we have that

$$E(\omega) = E_0 + E_1 \frac{i\omega\tau}{1 + i\omega\tau} \quad (1)$$

where  $E_1 = E_\infty - E_0$ , with  $E_0$  and  $E_\infty$  being the zero and high frequency elastic moduli, respectively. In rolling contacts such as that occurring in the RLRB between the rollers and the viscoelastic coating (see Figure 1c), the relative motion results in a cyclic deformation of the viscoelastic layer which, due to the viscoelastic response delay, may lead to asymmetric contact pressure distributions and, in turn, to a damping force  $F_d \propto \text{Im}[E(\omega)]$  opposing the relative motion [57, 59]. Notably, since  $\omega \approx \dot{z}/\lambda$ , we have that  $F_d = F_d(\dot{z}, \tau, \lambda)$ . Furthermore, from Eq. (1) we have that  $\text{Im}[E(\omega)]$  is maximum for  $\omega\tau \approx 1$ , thus the maximum damping force can be reasonably expected for  $\dot{z}^* \approx \lambda/\tau$ . Similarly, it can be shown that for very low and very high values of  $\dot{z}$ , the damping force vanishes, as  $\text{Im}[E(\omega \rightarrow 0)] = \text{Im}[E(\omega \rightarrow \infty)] = 0$ . However, in order to calculate the exact viscoelastic damping force as a function of  $\dot{z}$ , the contact problem between the rollers and the rubber layer has to be solved numerically, assuming both  $\lambda$  and  $\tau$  as a parameter. This can be done by relying on the boundary element formulation given in Refs. [60, 63], where the specific viscoelastic layer thickness  $h$  and roller

radius  $R$  are also taken into account.

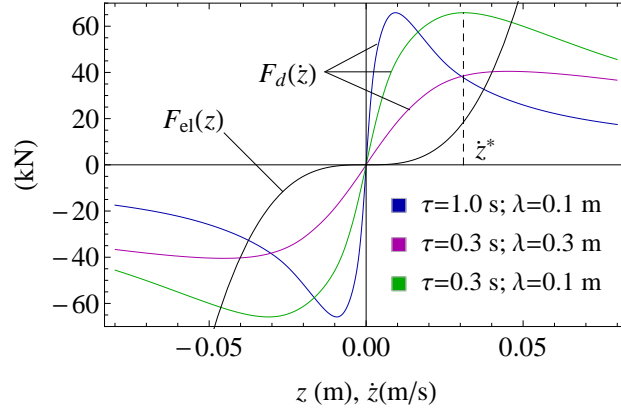


FIG. 2: The nonlinear elastic force  $F_{el}$  and damping force  $F_d$  as functions of the ground-RLRB relative displacement  $z$  and velocity  $\dot{z}$ , respectively. The damping force  $F_d$  is shown for different values of the viscoelastic material relaxation time  $\tau$  and contact wavelength  $\lambda$ . Results are for  $h/\lambda = 0.13$ .

In Figure 2 the trend the nonlinear forces  $F_{el}(z)$  and  $F_d(\dot{z})$  is shown. Interestingly, in the same figure the effect of the RLRB parameters  $\tau$  and  $\lambda$  on  $F_d$  can be appreciated: as indicated above, the ratio  $\tau/\lambda$  shifts the value of the peak velocity  $\dot{z}^*$ ; notably,  $\lambda$  also affects the peak amplitude. This is mainly due to the influence of  $\lambda$  on the mean contact pressure  $\bar{p}$  (i.e. on the amount of viscoelastic material cyclically deformed) which is given by the vertical static equilibrium of the rollers as

$$\bar{p} = g \frac{m_1 + m_2}{N\lambda b} \quad (2)$$

where  $g$  is the gravitational acceleration,  $b$  is the RLRB transverse width, and  $N$  is the number of rollers.

Finally, referring to the lumped scheme of Figure 1b, the linear momentum balance gives

$$\begin{aligned} m_1 (\ddot{x} + \ddot{z}) + \mu z^3 + F_d(\dot{z}) - k_s \zeta &= 0 \\ m_2 (\ddot{x} + \ddot{z} + \ddot{\zeta}) + k_s \zeta &= 0 \end{aligned} \quad (3)$$

with

$$\eta(t) = x(t) + z(t) + \zeta(t). \quad (4)$$

In order to integrate the set of nonlinear second order ODE of Eqs. (3), we adopted a fixed-step numerical strategy based on fourth order *Runge-Kutta* integration algorithm [65]. The choice of the integration time-step has followed a sensitivity analysis aiming at avoiding numerical instabilities.

Aiming at comparing the nonlinear system results in terms of dynamic response under periodic base excitation, a Duffing-like version of the system at hand (i.e.  $F_d = c_{eq}\dot{z}$  in Eq. (3)) is investigated by relying on the approximate *method of iterations* [66] (see Appendix A). Indeed, in agreement with Ref. [55], for each set of viscoelastic parameters ( $\tau$ ,  $\lambda$ ) a different damping curve exists (see Figure 2), and an equivalent linear damping coefficient  $c_{eq}$  can be defined as

$$c_{eq} = - \left. \frac{dF_d}{d\dot{z}} \right|_{\dot{z}=0} \quad (5)$$

Finally, it is noteworthy to observe that, according to Refs. [45, 60], viscoelastic calculations have been performed assuming steady rolling (i.e. constant velocity) between the RLRB rollers and the rubber layer, whereas periodic/seismic ground oscillation would reasonably induce reciprocating relative motion conditions. Nonetheless, as reported in Ref. [55], for  $a \ll s$  and  $\tau \ll T$ , with  $s$  and  $T$  being the stroke and period of the external forcing, steady sliding calculations can still provide a physically meaningful approximation of the real viscoelastic response.

### III. RESULTS

Calculations have been performed assuming an incompressible (i.e.  $\nu = 0.5$ ) viscoelastic material with a single relaxation time and  $E_0 = E_\infty/3 = 50$  MPa. Furthermore, in terms of RLRB geometry, we assumed  $h/\lambda = 0.13$ ,  $R/\lambda = 0.3$ , and  $b = 1$  m.

Since RLRBs are usually employed in the isolation of buildings such as hospitals, schools and museums [12], we assumed the dynamic model parameters in order to achieve a qualitative overlap with these possible applications. Indeed, according to Ref. [55], we set  $m_1 = 1 \times 10^2$  kg,  $m_2 = 1 \times 10^5$  kg. The supporting beam stiffness has been estimated as the bending stiffness of a commercial HEB 300 steel beam, with  $L = 3$  m, thus resulting in  $k_s = 6 \times 10^6$  N/m. Finally, to simplify the results reading, the nonlinear stiffness will be written as  $\mu = \mu_0 6.2 \times 10^7 \text{N/m}^3$ , with  $\mu_0$  being a dimensionless coefficient.

#### A. Periodic dynamics

In this section we focus on the dynamic response of the physical system under periodic base excitation in the form  $x(t) = x_0 \sin(\omega t)$ . Since the system is nonlinear both in terms of stiffness and damping, we expect the dynamic behavior to be affected by the initial conditions; therefore, we numerically simulate both forward and backward excitation frequency sweep, for different values of both the excitation amplitude  $x_0$  and damping conditions.

The frequency response is shown in Figures 3 in terms of the amplitude of both the inertial mass oscillation  $\eta_m$  (upper diagrams) and the relative velocity between the ground and RLRB  $\dot{z}_m$  (lower diagrams). Specifically, Figure 3a refers to a sufficiently small value of  $x_0$ . The equivalent Duffing-like system with linear damping (black curve) shows the well-known stiffening multivalued frequency response (black curve), which overhangs to the high-frequency side, thus leading to a bistable region. Under these conditions, since  $\dot{z}_m/\dot{z}^* < 1$ , the system equipped with the RLRB is poorly affected by the damping nonlinearity, thus a slightly less damped response is observed (see blue and red curves in Figure 3a) associated to an overall larger oscillation amplitude compared to the Duffing-like system. Although in Figure 3b different parameters for damping and excitation amplitude are investigated, the physical scenario described above still qualitatively applies. Nonetheless, this time significantly larger values of  $\eta$  are expected, as forward swapping results show fast increasing oscillation amplitudes, eventually approaching the vertical asymptote at  $\omega_1 \approx 7.75$  rad/s (see Appendix A). Beyond this threshold, single-valued results are recovered, with forward and backward stable points overlapping. A similar behavior is observed in the lower diagram of Figure 3b concerning the amplitude of  $\dot{z}$ . In Figure 3c a dramatically different system response is observed. Indeed, contrary to the cases discussed above, this time significant differences are reported between the Duffing-like system behavior and the RLRB. Specifi-

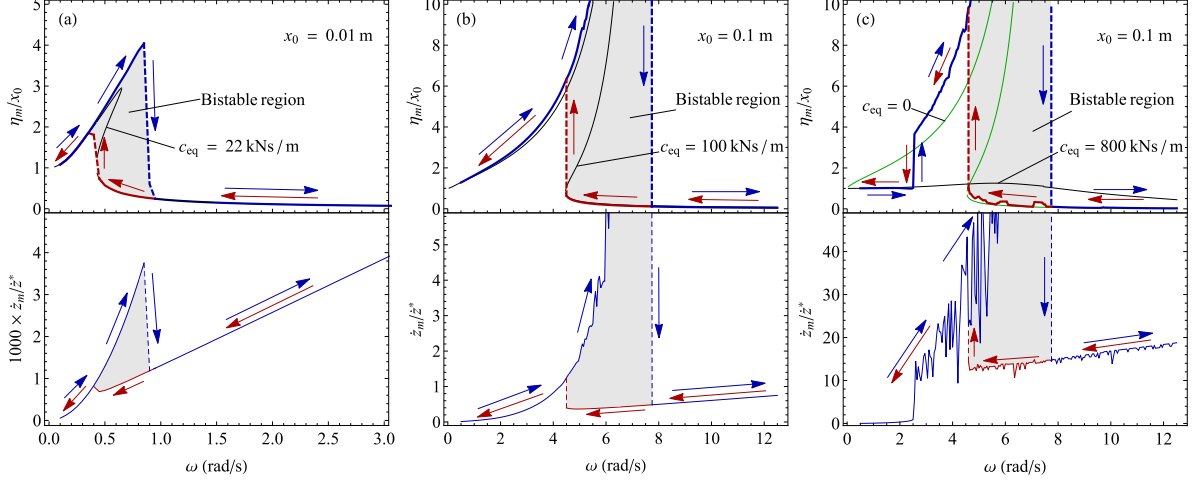


FIG. 3: The normalized amplitude of the inertial mass oscillation  $\eta_m/x_0$  (upper diagrams) and the relative velocity amplitude  $\dot{z}_m/\dot{z}^*$  between the ground and RLRB (lower diagrams) as a function of the excitation frequency  $\omega$ . Blue and red curves represent forward and backward frequency sweep stable results for the nonlinear system, respectively. Black curves represent equivalent Duffing-like approximate results, whereas the green curve is the undamped approximate result. The dimensionless nonlinear stiffness is  $\mu_0 = 1$ , and the nonlinear damping parameters are  $\lambda = 0.2$  m and (a)  $\tau = 0.002$  s, (b)  $\tau = 0.0095$  s, (c)  $\tau = 0.0742$  s.

cally, this time, the choice of  $\tau$  and  $\lambda$  leads to equivalent larger damping (i.e. lower value of  $\dot{z}^*$ ) entailing more severe peak velocity overcoming, as indicated by the lower diagram where  $\dot{z}_m/\dot{z}^* \gg 1$ . Under these conditions, the nonlinear system is able to replicate the highly damped Duffing-like results only at low excitation frequency, whereas the qualitative agreement is lost at larger  $\omega$ . In the same figure, the undamped system behavior is reported for comparison (i.e.  $F_d = 0$  in Eq. (3)). Focusing on the upper overhanging branch, the undamped system present even lower amplitudes than the nonlinearly damped one. Such a result is peculiar of system presenting portions of the damping curve decreasing with increasing velocity such as those based on viscoelastic friction. In this case, indeed, the abrupt decrease of the damping force for  $|\dot{z}(t)| > \dot{z}^*$  generates additional self-excited components to the system vibrational response. Notably, the occurrence of such a phenomenon is mostly governed by the sharpness of the damping force decrease beyond the peak, thus resulting noteworthy in our system only at sufficiently large values of  $c_{eq}$  (see Figure 2).

Such a result is also confirmed by Figures 4 where the spectrogram of the oscillation amplitude  $\eta$  is shown. Specifically, Figure 4a refers to the backward stable branch of Figure 3b. As expected, in this case the main spectral contribution is associated to the external excitation frequency, whereas different spectral components are negligible except in the proximity of the solution jump up ( $\omega \approx 4.5$  rad/s). Similarly, Figure 4b refers to the backward stable branch of Figure 3c. Interestingly, a significant spread of the spectrum is associated to the peak velocity overcoming, consistently with the activation of additional self-excited vibration components.

Figures 5 show the inertial mass oscillation time history (left column) and phase portrait (right column) at different values of  $\omega$  on the backward branch of Figure 3c. Figures 5a-b and 5g-h share the same solution with the equivalent Duffing-like system with linear damping,

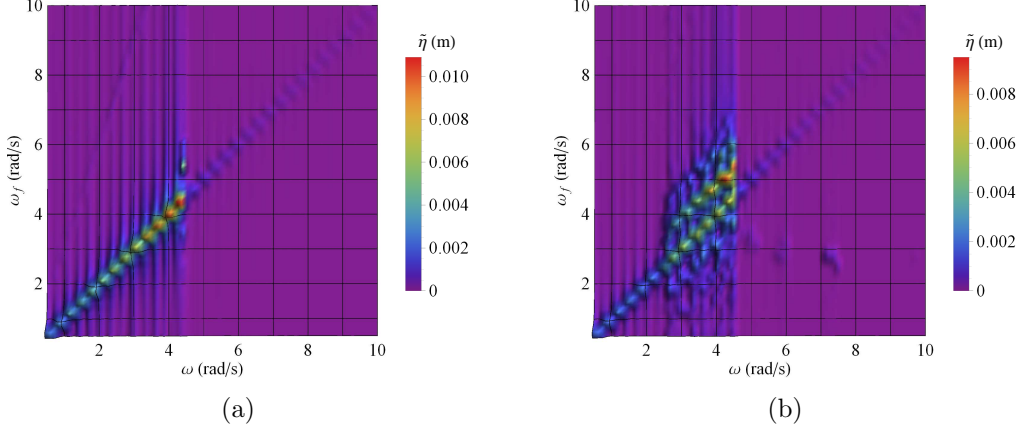


FIG. 4: The spectrograms of the oscillation amplitude  $\tilde{\eta}$  vs the periodic excitation frequency  $\omega$  for the backward stable branches of (a) Figure 3b, and (b) Figure 3c. Results are for  $x_0 = 0.1$  m,  $\mu_0 = 1$ ,  $\lambda = 0.2$  m and (a)  $\tau = 0.0095$  s, (b)  $\tau = 0.0742$  s.

thus showing a periodic response with elliptical phase portrait due to the slight damping nonlinearity. On the contrary, Figures 5c-d show different results as, this time, due to the system nonlinearity additional frequencies are excited, as indeed shown by the phase portrait where at least five closed paths can be observed. Finally, the responses shown in Figures 5e-f is even more complex, involving an larger number of spectral components.

## B. Seismic dynamics

The fundamental investigation performed in the previous section allows to conclude that the nonlinear isolator under investigation can exhibit significantly different dynamic behaviors depending on the value of the elastic ( $\mu$ ) and damping ( $\tau, \lambda$ ) parameters.

In terms of seismic vibration mitigation, in Ref. [55], the performance of an RLRB equipped with linear stiffness has been compared to a generic linear isolator on a single seismic event, showing a marked ability of the RLRB with linear stiffness to relief the loads acting on the superstructure. However, since the possible excitation spectrum in real applications (e.g. earthquakes, wind, failures) is often unknown, we expect the robustness of the isolation performance to play a key role in practical problems. Therefore, focusing on the RLRB with nonlinear damping and stiffness and the generic linear isolator, we perform a global optimization of both the system assuming a series of five different seismic events as inputs; then, we compare the specific isolation performance achieved by both systems in global optimum conditions on each specific shock. To this regard, the linear momentum balance for the generic linear system can be achieved as the linearized version of Eqs. (3), so

$$\begin{aligned} m_1 (\ddot{x} + \ddot{z}_l) + k_l z_l + c_l \dot{z}_l - k_s \zeta_l &= 0 \\ m_2 (\ddot{x} + \ddot{z}_l + \ddot{\zeta}_l) + k_s \zeta_l &= 0 \end{aligned} \quad (6)$$

where the optimization parameters are  $c_l$  and  $k_l$ .

Furthermore, since our study focus on a simple single-story superstructure, most of the usual performance index [68, 70], based on inter-story drift and shear stresses, cannot be adopted. However, according to Refs. [69, 71], for each considered shock we can define



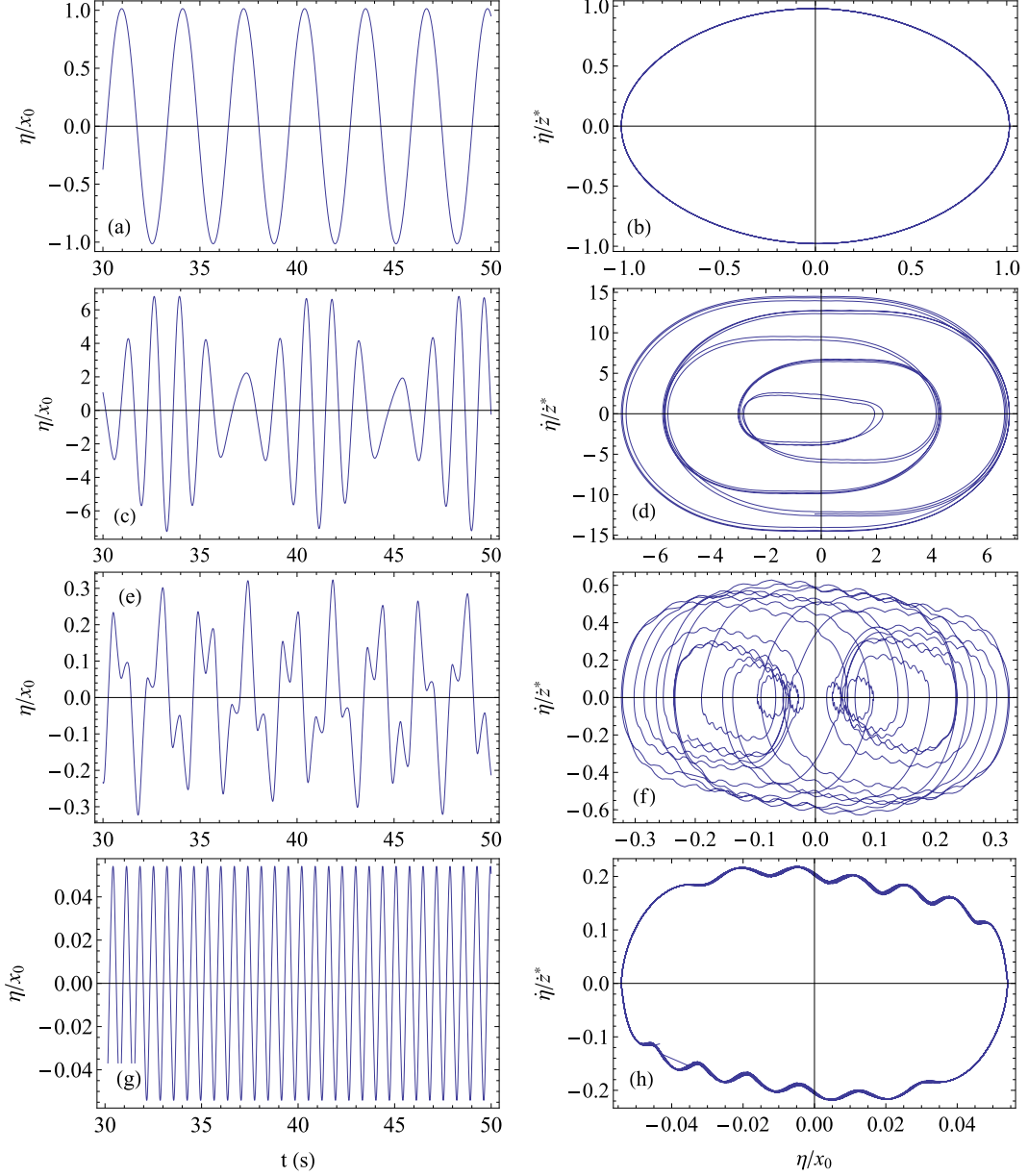


FIG. 5: The time history of the normalized displacement  $\eta/x_0$  (left column), and the normalized phase-diagram (right column). Data refer to the backward stable branch of Figure 3c, with  $\omega = 2$  rad/s (a-b); 4 rad/s (c-d); 7.2 rad/s (e-f); 9 rad/s (g-h).

three main source of damage: (i) the amplitude  $F_m$  of the inertial force acting on the mass  $m_2$  (i.e.  $F_m = k_s \zeta_m$  with  $\zeta_m$  being the amplitude of  $\zeta$ ), associated to the superstructure instantaneous damage; (ii) the root mean square  $F_{rms}$  of the inertial force acting on the mass  $m_2$  (i.e.  $F_{rms} = k_s/T [\int_T \zeta^2(t) dt]^{1/2}$  with  $T$  being the shock duration), associated to the material hysteresis and fatigue; (iii) the amplitude of the relative displacement at the base  $z_m$ , associated to possible compatibility issues with surrounding systems (e.g. buildings,

pipng, frameworks). Finally, the performance index is defined as

$$\varphi = \frac{1}{n} \sum_{k=1}^n \left( w_1 \frac{F_{m,k}}{F_{m,0}} + w_2 \frac{F_{rms,k}}{F_{rms,0}} + w_3 \frac{z_{m,k}}{z_{m,0}} \right) \quad (7)$$

where  $k$  spans through the  $n$  seismic events, and  $w_i$ , with  $i = 1, 2, 3$ , are weighting terms. In our analysis we assume  $w_i = 1/3$ . Notably, the smaller the value of  $\varphi$ , the better the performance is. Moreover, in Eq. (7)  $F_{m,0}$ ,  $F_{rms,0}$ , and  $z_{m,0}$  are homogenization terms defined as the absolute maxima of the corresponding quantities in the investigated domain. The optimization process has been solved by means of a brute-force search with structured sampling of the parameters domain.

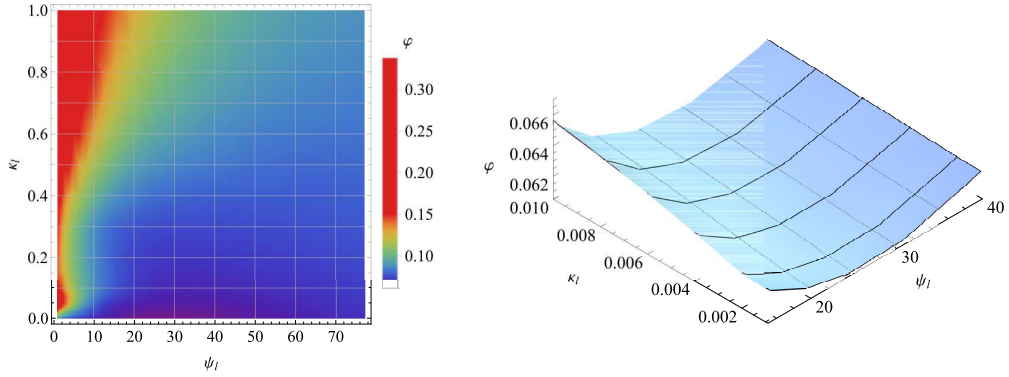


FIG. 6: The performance index  $\varphi$  of the system equipped with generic linear isolator as a function of the dimensionless linear stiffness  $\kappa_l$  and damping  $\psi_l$  (left), with a close up to the optimal region (right). With reference to Eqs. (6),  $k_l = \kappa_l \times 3.1 \times 10^6 \text{N/m}$  and  $c_l = \psi_l \times 10^4 \text{Nm/s}$ .

Figures 6 show the effect of dimensionless base stiffness ( $\kappa_l$ ) and damping ( $\psi_l$ ) on the response of the system equipped with a generic linear isolator. Interestingly, the base stiffness appears less effective than the damping coefficient in determining the overall isolation performance, thus the investigated range of stiffness has been cropped at reasonably low values.

Similarly, Figures 7 show the isolation performance of the system equipped with RLRB and nonlinear stiffness. For what concerns the damping behavior, as expected from the discussion reported in the previous sections, we observe a slightly larger effect of  $\tau$  on the overall isolation performance, compared to  $\lambda$ . The reason of such a behavior can be ascribed to the direct effect of  $\tau$  and the slope of the damping curve, contrary to  $\lambda$  which also affects the damping force peak value. For what concerns the nonlinear elastic term, although the optimum condition is related to sufficiently low values of  $\mu_0$ , it is noteworthy to observe that a non-monotonic effect on the overall isolation performance occurs.

The isolation performance in global optimum conditions are reported in Table I, showing that, for each of the considered shocks, the nonlinear RLRB is able to provide better loads isolation in a wider range of excitation spectra (i.e. for different seismic events). Such result seems to indicate a higher performance robustness associated to the nonlinear isolation with respect to the excitation variability, with direct possible impact on several engineering applications in which the forcing spectrum is unknown and blind design of the isolation is required.

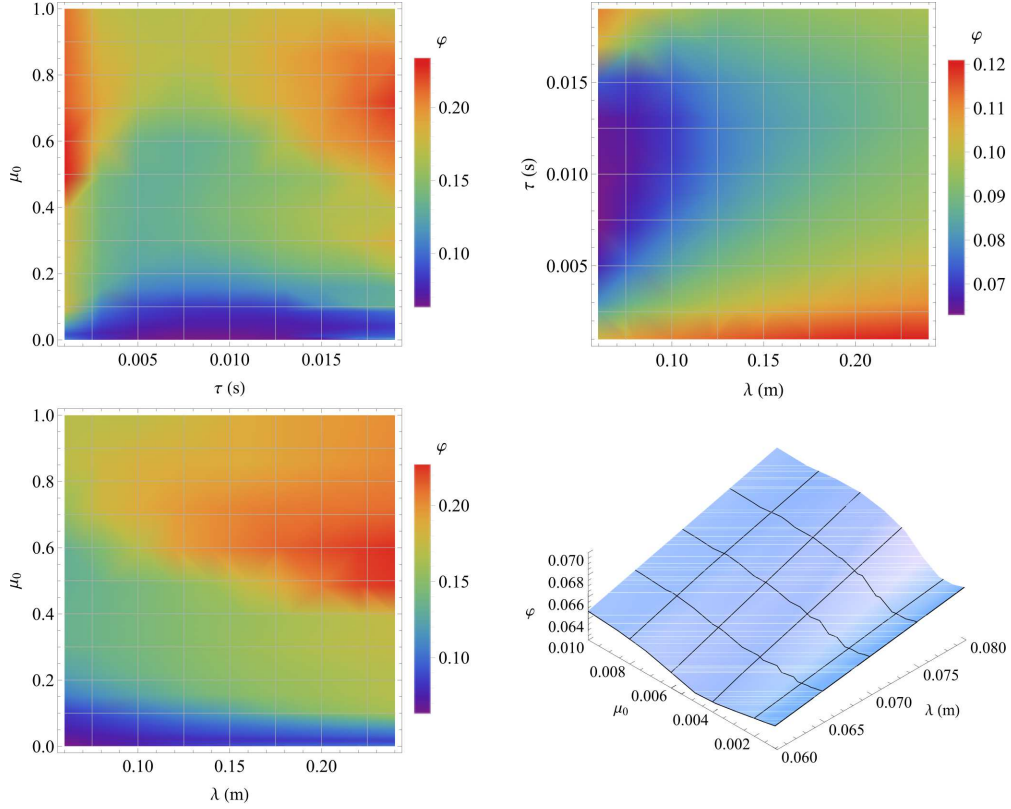


FIG. 7: The performance index  $\varphi$  of the system equipped with nonlinear RLRB as a function of the dimensionless nonlinear elastic  $\mu_0$  term, and the RLRB damping parameters  $\lambda$  and  $\tau$ . A 3D closeup to the optimal region is also provided.

	Linear			Nonlinear		
	$F_m^i$ (kN)	$F_{rms}^i$ (kN)	$z_m$ (cm)	$F_m^i$ (kN)	$F_{rms}^i$ (kN)	$z_m$ (cm)
Irpinia 1980	92.7	15.3	19.5	66.3	13.2	23.9
Izmit 1999	102	15.5	28.3	69.4	14.2	36.7
Waiau 2016	245	22.9	16.8	81.1	16.5	23.9
Kathmandu 2015	103	20.2	31.2	100	21.0	57.7
Christchurch 2010	223	31.3	25.5	89.4	21.0	40.4
Mean	153	21.0	24.6	81.2	17.2	36.5
Standard deviation	74.3	6.58	6.0	14	3.69	14.0

TABLE I: Optimization results for both the nonlinear and linear system performance. Optimal conditions are  $\kappa_l = 0.001$  and  $\psi_l = 24.59$  for the linear system, and  $\mu_0 = 0.0048$ ,  $\lambda = 0.06$  m,  $\tau = 0.007$  s in the nonlinear case.

The optimal time histories of  $\eta$  are shown in the left column in Figures 8 for all the seismic events here considered. We observe that, in most of the cases, the nonlinear RLRB base isolation leads to overall smoother responses compared to a generic linear base isolation, also slightly reducing the peak displacement. Interestingly, a persisting displacement offset may be observed after the shock between the superstructure and the ground in the case of nonlinear RLRB. This has to be ascribed to the slowly decaying  $z$  relative rigid

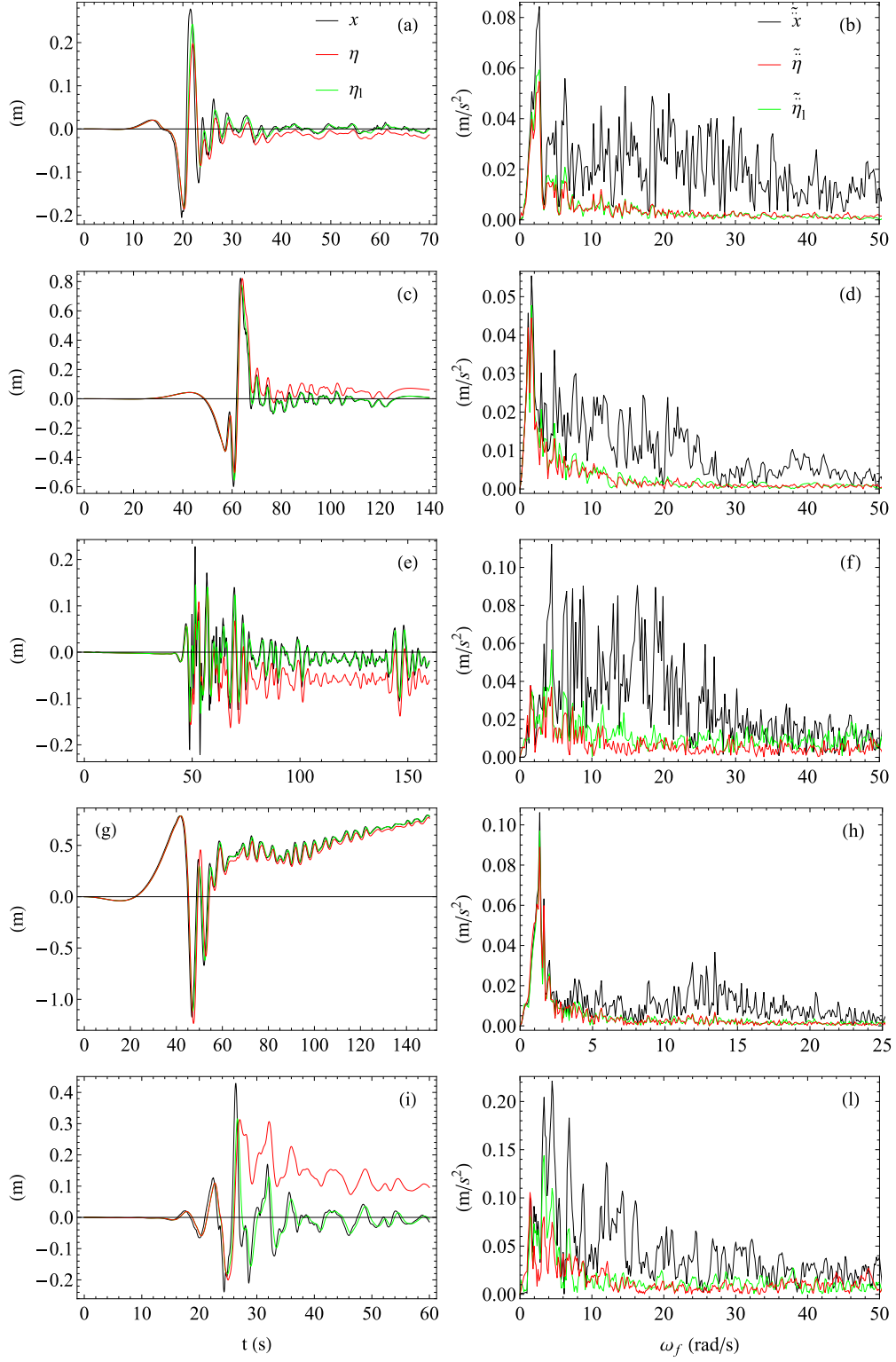


FIG. 8: The time history (left column) and spectral components (right column) of the optimal responses of the system equipped with generic linear base isolation (green curves) and nonlinear RLRB (red curves) to the considered earthquake shocks: Irpinia 1980 (a-b); Izmit 1999 (c-d); Waiiau 2016 (e-f); Kathmandu 2015 (g-h); Christchurch 2010 (i-l).

displacement between the superstructure base and the ground due to the poor re-centering effect provided by the nonlinear base elastic term for  $z \ll 1$ . Of course, this displacement offset asymptotically vanishes in the long term response. Similar conclusions can be drawn from the right column in Figures 8 showing the spectral representation of the inertial mass acceleration  $\ddot{\eta}$ . As expected, both the linear and nonlinear base isolation systems behave as low pass filters, however enhanced filtering performances are associated to the nonlinear RLRB.

#### IV. CONCLUSIONS

In this work, nonlinear viscoelastic vibrations are investigated with specific focus on nonlinear damping behavior arising in viscoelastic rolling contacts such as those involved in RLRB base insulation systems.

We found that, due to the bell-shaped damping curve peculiar of viscoelastic materials, different dynamic regimes can be observed under periodic loading, sometimes triggering self-excited vibrational components, with higher oscillation amplitudes compared to equivalent systems with linear damping.

Furthermore, we compare the effectiveness of the RLRB equipped with cubic spring in terms of real seismic base isolation against a generic linear isolator. We performed global optimization on damping and stiffness parameters in both cases assuming as inputs a set of five different seismic events. Results highlight a better loads isolation performance of the nonlinear RLRB, clearly showing that under the same global optimal conditions the nonlinear base isolation is able to tolerate a wider range of excitations, thus exhibiting a significantly more robust performance than the linear one. This suggests that nonlinear isolation systems involving non-monotonic damping, such as those based on viscoelastic friction, may represent a preferable choice in applications requiring blind design of the isolation system.

**Acknowledgement 1** *This project has received funding from the European Union’s Horizon 2020 research and innovation programme under the Marie Skłodowska-Curie grant agreement No 845756 (N.M. Individual Fellowship). This work was partly supported by the Italian Ministry of Education, University and Research under the Programme “Progetti di Rilevante Interesse Nazionale (PRIN)”, Grant Protocol 2017948, Title: Foam Airless Spoked Tire – FASTire (G.C.).*

#### Appendix A: Duffing-like system approximate frequency response

Here we report the method [66] we adopted to calculate the approximated frequency response of the Duffing-like two-DoF system with nonlinear elastic force  $\mu x^3$  and linear (viscous) damping  $c\dot{x}$ . We focus on the case with periodic ground excitation in the form  $x(t) = x_0 \cos \omega t$ . The linear momentum balance equations are

$$\begin{aligned} m_1 \ddot{z} &= -\mu z^3 - c\dot{z} + k_s \zeta + m_1 x_0 \omega^2 \cos \omega t \\ m_2 \ddot{\zeta} + m_2 \ddot{z} &= -k_s \zeta + m_2 x_0 \omega^2 \cos \omega t \end{aligned} \tag{A1}$$

The system is nonautonomous as the time  $t$  appears explicitly in the forcing terms. We seek only the steady state harmonic solution by the method of iteration. The first assumed solution is

$$\begin{aligned} z &= A_1 \cos \omega t + A_2 \sin \omega t \\ \zeta &= B_1 \cos \omega t + B_2 \sin \omega t \end{aligned} \quad (\text{A2})$$

By substituting eq. (A2) into the differential equations (A1), we found that

$$\begin{aligned} z &= \frac{1}{36m_1\omega^2} [36m_1\omega^2 (c_1 + c_2t) + 9 (-4B_1k_s + 3\mu A_1^3 + 3\mu A_1A_2^2 + 4c\omega A_2 - 4m_1\omega^2 x_0) \cos \omega t + \\ &\mu A_1 (A_1^2 - 3A_2^2) \cos 3\omega t + 9 (-4B_2k_s + 3\mu A_1^2A_2 + 3\mu A_2^3 - 4A_1c\omega) \sin \omega t - \\ &\mu A_2 (A_2^2 - 3A_1^2) \sin 3\omega t] \end{aligned} \quad (\text{A3})$$

$$\begin{aligned} \zeta &= \frac{1}{36m_1m_2\omega^2} \{36m_1m_2\omega^2 (c_3 + c_4t) + 9[4B_1k_s (m_1 + m_2) - 3\mu m_2A_1 (A_1^2 + A_2^2) - \\ &4A_2m_2c\omega] \cos \omega t - \mu A_1m_2 (A_1^2 - 3A_2^2) \cos 3\omega t + 9[4B_2k_s (m_1 + m_2) \\ &- 3\mu A_2m_2 (A_1^2 + A_2^2) + 4A_1m_2c\omega] \sin \omega t + \mu m_2A_2 (A_2^2 - 3A_1^2) \sin 3\omega t\} \end{aligned} \quad (\text{A4})$$

Since we focus on the harmonic solution with period  $T = 2\pi/\omega$ , we have that  $c_1 = c_2 = c_3 = c_4 = 0$ . Indeed, we only aim at providing a qualitative estimation of the overall dynamic behavior, here we neglect the higher harmonic terms. However, the method can easily be further iterated.

Collecting all the trigonometric terms in Eqs. (A3,A4) and considering Eqs. (A2), the following set of nonlinear algebraic equations is found

$$\begin{aligned} A_1 &= \frac{1}{4m_1\omega^2} [-4B_1k_s + 3\mu A_1^3 + 3\mu A_1A_2^2 + 4A_2c\omega - 4m_1\omega^2 x_0] \\ A_2 &= \frac{1}{4m_1\omega^2} [-4B_2k_s + 3\mu A_1^2A_2 + 3\mu A_2^3 - 4A_1c\omega] \\ B_1 &= \frac{1}{4m_1m_2\omega^2} [4B_1k_s(m_1 + m_2) - 3\mu A_1m_2(A_1^2 + A_2^2) - 4A_2m_2c\omega] \\ B_2 &= \frac{1}{4m_1m_2\omega^2} [4B_2k_s(m_1 + m_2) - 3\mu A_2m_2(A_1^2 + A_2^2) + 4A_1m_2c\omega] \end{aligned} \quad (\text{A5})$$

which can be solved for  $A_1(\omega)$ ,  $A_2(\omega)$ ,  $B_1(\omega)$ ,  $B_2(\omega)$ . Finally, the amplitude of the oscillation of inertial mass is calculated as

$$\eta_{m,0}(\omega) = \sqrt{(A_1 + B_1 + x_0)^2 + (A_2 + B_2)^2} \quad (\text{A6})$$

Figures 9 show the frequency response of the Duffing-like system under different damping conditions.

- 
- [1] Rahman, Mahmudur, et al. "Performance enhancement of wind turbine systems with vibration control: A review." *Renewable and Sustainable Energy Reviews* 51 (2015): 43-54.

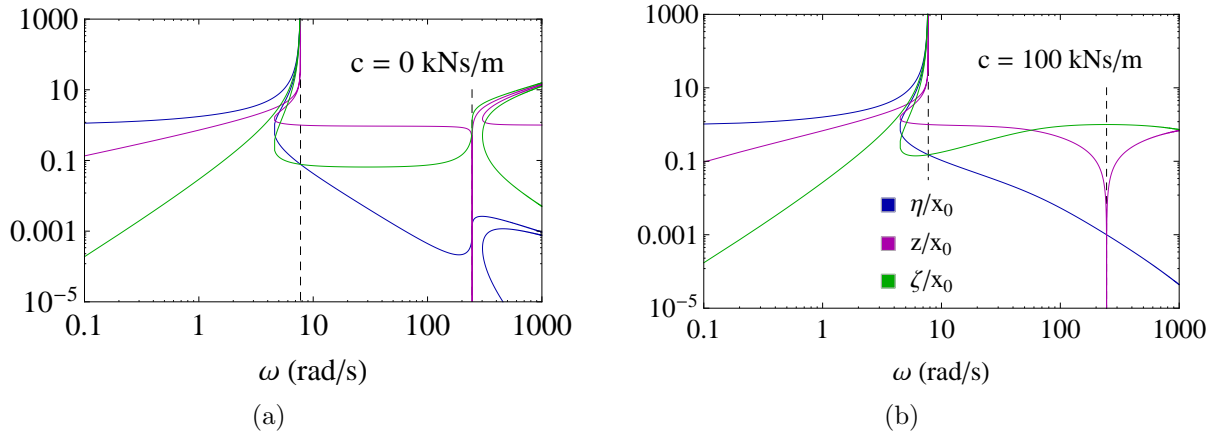


FIG. 9: The frequency response of  $\eta$ ,  $z$ , and  $\zeta$  under undamped (a) and damped conditions (b). Results are for  $x_0 = 0.1\text{m}$ . The two dashed asymptotes are at  $\omega_1 = \sqrt{k_s/m_2}$  and  $\omega_2 = \sqrt{k_s/m_1}$

- [2] Zuo, Haoran, Kaiming Bi, and Hong Hao. "Using multiple tuned mass dampers to control offshore wind turbine vibrations under multiple hazards." *Engineering Structures* 141 (2017): 303-315.
- [3] Chen, Junling, and Christos T. Georgakis. "Tuned rolling-ball dampers for vibration control in wind turbines." *Journal of Sound and Vibration* 332.21 (2013): 5271-5282.
- [4] Jie, Li, Zhang Zili, and Chen Jianbing. "Experimental study on vibration control of offshore wind turbines using a ball vibration absorber." *Energy and Power Engineering* 2012 (2012).
- [5] Colwell, Shane, and Biswajit Basu. "Tuned liquid column dampers in offshore wind turbines for structural control." *Engineering Structures* 31.2 (2009): 358-368.
- [6] Zhang, Zili, et al. "Performance evaluation of full-scale tuned liquid dampers (TLDs) for vibration control of large wind turbines using real-time hybrid testing." *Engineering Structures* 126 (2016): 417-431.
- [7] Maldonado, Victor, et al. "Active Vibration Control of a Wind Turbine Blade Using Synthetic Jets." *International Journal of Flow Control* 1.4 (2009).
- [8] Daley, S., I. Zazas, and J. Hatonen. "Harmonic control of a 'smart spring' machinery vibration isolation system." *Proceedings of the Institution of Mechanical Engineers, Part M: Journal of Engineering for the Maritime Environment* 222.2 (2008): 109-119.
- [9] Rivin, Eugene I. "Vibration isolation of precision equipment." *Precision Engineering* 17.1 (1995): 41-56.
- [10] Nieto, A. J., et al. "Unbalanced machinery vibration isolation with a semi-active pneumatic suspension." *Journal of sound and vibration* 329.1 (2010): 3-12.
- [11] Farshidianfar, A., Saghafi, A., Kalami, S. M., & Saghafi, I. (2012). Active vibration isolation of machinery and sensitive equipment using H $\infty$  control criterion and particle swarm optimization method. *Meccanica*, 47(2), 437-453.
- [12] B. Myslimaj, S. Gamble, D. Chin-Quee, A. Davies, B. Breukelman. Base isolation technologies for seismic protection of museum artifacts. In *The 2003 IAMFA Annual Conference in San Francisco, California*. San Francisco, CA: IAMFA.

- [13] S.T. De la Cruz, F. López-Almansa, S. Oller. Numerical simulation of the seismic behavior of building structures equipped with friction energy dissipators. *Comput Struct*, 85 (2007) 30-42.
- [14] D. Foti, M. Diaferio, R. Nobile. Dynamic behavior of new aluminum–steel energy dissipating devices. *Struct Control Hlth*, 20 (2013) 1106-1119.
- [15] P.S. Harvey Jr, K.C. Kelly. A review of rolling-type seismic isolation: Historical development and future directions. *Eng Struct*, 125 (2016) 521-531.
- [16] P.S. Harvey Jr, H.P. Gavin. Assessment of a rolling isolation system using reduced order structural models. *Eng Struct*, 99 (2015) 708-725.
- [17] C.D. Casey, P.S. Harvey Jr, W. Song. Multi-unit rolling isolation system arrays: Analytical model and sensitivity analysis. *Eng Struct*, 173 (2018) 656-668.
- [18] Y. Starosvetsky, O.V. Gendelman. Vibration absorption in systems with a nonlinear energy sink: nonlinear damping. *J Sound Vib*, 324 (2009) 916-939.
- [19] O.V. Gendelman, A. Alloni. Dynamics of forced system with vibro-impact energy sink. *J Sound Vib*, 358 (2015) 301-314.
- [20] Pazooki, A., Goodarzi, A., Khajepour, A., Soltani, A., & Porlier, C. (2018). A novel approach for the design and analysis of nonlinear dampers for automotive suspensions. *Journal of Vibration and Control*, 24(14), 3132-3147.
- [21] Lu, Zheng, et al. "Nonlinear dissipative devices in structural vibration control: A review." *Journal of Sound and Vibration* 423 (2018): 18-49.
- [22] Nucera, F., Iacono, F. L., McFarland, D. M., Bergman, L. A., & Vakakis, A. F. (2008). Application of broadband nonlinear targeted energy transfers for seismic mitigation of a shear frame: Experimental results. *Journal of sound and vibration*, 313(1-2), 57-76.
- [23] Wierschem, N. E., Hubbard, S. A., Luo, J., Fahnestock, L. A., Spencer, B. F., McFarland, D. M., ... & Bergman, L. A. (2017). Response attenuation in a large-scale structure subjected to blast excitation utilizing a system of essentially nonlinear vibration absorbers. *Journal of Sound and Vibration*, 389, 52-72.
- [24] Wang, J., Wierschem, N., Spencer Jr, B. F., & Lu, X. (2015). Experimental study of track nonlinear energy sinks for dynamic response reduction. *Engineering Structures*, 94, 9-15.
- [25] Tian, L., Rong, K., Zhang, P., & Liu, Y. (2017). Vibration control of a power transmission tower with pounding tuned mass damper under multi-component seismic excitations. *Applied Sciences*, 7(5), 477.
- [26] Nakamura, Y., & Watanabe, K. (2016). Effects of balanced impact damper in structures subjected to walking and vertical seismic excitations. *Earthquake engineering & structural dynamics*, 45(1), 113-128.
- [27] Lee, Y. S., Vakakis, A. F., Bergman, L. A., McFarland, D. M., & Kerschen, G. (2007). Suppression aeroelastic instability using broadband passive targeted energy transfers, part 1: Theory. *AIAA journal*, 45(3), 693-711.
- [28] Lee, Y. S., Kerschen, G., McFarland, D. M., Hill, W. J., Nickkawde, C., Strganac, T. W., ... & Vakakis, A. F. (2007). Suppressing aeroelastic instability using broadband passive targeted energy transfers, part 2: experiments. *AIAA journal*, 45(10), 2391-2400.
- [29] Kushida, Y., Hara, S., Otsuki, M., Yamada, Y., Hashimoto, T., & Kubota, T. (2013). Robust landing gear system based on a hybrid momentum exchange impact damper. *Journal of Guidance, Control, and Dynamics*, 36(3), 776-789.
- [30] Ahmad, N., Ranganath, R., & Ghosal, A. (2017). Modeling and experimental study of a honeycomb beam filled with damping particles. *Journal of Sound and Vibration*, 391, 20-34.
- [31] Gourc, E., Seguy, S., Michon, G., & Berlioz, A. (2013). Chatter control in turning process



- with a nonlinear energy sink. In *Advanced Materials Research* (Vol. 698, pp. 89-98). Trans Tech Publications Ltd.
- [32] Gourc, E., Seguy, S., Michon, G., Berlioz, A., & Mann, B. P. (2015). Quenching chatter instability in turning process with a vibro-impact nonlinear energy sink. *Journal of Sound and Vibration*, 355, 392-406.
  - [33] Ema, S., & Marui, E. (2000). Suppression of chatter vibration of boring tools using impact dampers. *International Journal of Machine Tools and Manufacture*, 40(8), 1141-1156.
  - [34] Samani, F. S., & Pellicano, F. (2012). Vibration reduction of beams under successive traveling loads by means of linear and nonlinear dynamic absorbers. *Journal of Sound and Vibration*, 331(10), 2272-2290.
  - [35] Xiao, W., Li, J., Wang, S., & Fang, X. (2016). Study on vibration suppression based on particle damping in centrifugal field of gear transmission. *Journal of Sound and Vibration*, 366, 62-80.
  - [36] Tian, L., & Gai, X. (2015). Wind-induced vibration control of power transmission tower using pounding tuned mass damper. *Journal of Vibroengineering*, 17(7), 3693-3701.
  - [37] Fu, X., Li, H. N., Li, J. X., & Zhang, P. (2017). A pounding spacer damper and its application on transmission line subjected to fluctuat
  - [38] Jo, I., Kaneko, T., Nagatsu, S., Takahashi, C., & Kimura, M. (1989). Development of highway light pole with resistance to wind vortex-induced oscillations. *Kawasaki Steel Technical Report*, 21.
  - [39] M.A. Bukhari, O. Barry, E. Tanbour. On the vibration analysis of power lines with moving dampers. *J Vib Control*, 24 (2018) 4096-4109.
  - [40] Symans, M. D., Charney, F. A., Whittaker, A. S., Constantinou, M. C., Kircher, C. A., Johnson, M. W., & McNamara, R. J. (2008). Energy dissipation systems for seismic applications: current practice and recent developments. *Journal of structural engineering*, 134(1), 3-21.
  - [41] Constantinou, M. C., & Symans, M. D. (1993). Experimental study of seismic response of buildings with supplemental fluid dampers. *The Structural Design of Tall Buildings*, 2(2), 93-132.
  - [42] Lee, D., & Taylor, D. P. (2001). Viscous damper development and future trends. *The Structural Design of Tall Buildings*, 10(5), 311-320.
  - [43] Lu, X., Zhou, Y., & Yan, F. (2008). Shaking table test and numerical analysis of RC frames with viscous wall dampers. *Journal of structural engineering*, 134(1), 64-76.
  - [44] Lin, Y. Y., Chang, K. C., & Chen, C. Y. (2008). Direct displacement-based design for seismic retrofit of existing buildings using nonlinear viscous dampers. *Bulletin of Earthquake Engineering*, 6(3), 535-552.
  - [45] N. Menga, D. Foti, G. Carbone. Viscoelastic frictional properties of rubber-layer roller bearings (RLRB) seismic isolators. *Meccanica*, 52 (2017), 2807-2817.
  - [46] D. Foti, J.M. Kelly Experimental analysis of a model isolated at the base with rubber-layer roller bearing (RLRB). *Euro Earthquake Eng*, 10 (1996) 3-13.
  - [47] M. Mezzina, D. Raffaele, C. Dentamaro, D. Foti, P. Monaco. Seismic isolation with RLRB (Rubber Layer Roller Bearing), *Proc. of the 1st European conference on Structural control*; Barcelona, Spain, May 29-31, (1996) 459-466.
  - [48] A.H.Muhr, M. Sulong, A.G. Thomas. Rolling-ball rubber-layer isolators. *J Nat Rubber Res*, 12 (1997) 199-214.
  - [49] A.H.Muhr, G. Bergamo. Shaking table tests on rolling-ball rubber-layer isolation system. In: *14th European conference on earthquake engineering*. (2010) 5703-5710.

- [50] L. Guerreiro, J. Azevedo, A.H. Muhr. Seismic tests and numerical modeling of a rolling-ball isolation system. *J of Earthq Eng*, 11 (2007), 49-66.
- [51] D. Foti, A. Catalan Goni, S. Vacca. On the dynamic response of rolling base isolation systems. *Struct Control Hlth*, 20 (2013) 639–48. <http://dx.doi.org/10.1002/stc.1538>.
- [52] D. Foti, Isolatore sismico (Seismic Isolator), Italian Patent 0001414213, 2015
- [53] D. Foti, (2019). Rolling devices for seismic isolation of lightweight structures and equipment. Design and realization of a prototype. *Struct Control Hlth*, 26, e2311.
- [54] F. Mazza. Seismic demand of base-isolated irregular structures subjected to pulse-type earthquakes. *Soil Dyn Earthq Eng*, 108 (2018) 111-129.
- [55] Menga, N., F. Bottiglionne, and G. Carbone. "The nonlinear dynamic behavior of a Rubber-Layer Roller Bearing (RLRB) for vibration isolation." *Journal of Sound and Vibration* 463 (2019): 114952.
- [56] Shinozuka, M., & Deodatis, G. (1988). Stochastic process models for earthquake ground motion. *Probabilistic engineering mechanics*, 3(3), 114-123.
- [57] Christensen R. M., *Theory of viscoelasticity*, Academic Press, New York, 1982.
- [58] G. Carbone, L. Mangialardi. Analysis of the adhesive contact of confined layers by using a Green's function approach. *J Mech Phys Solids*, 56 (2008) 684-706.
- [59] N. Menga, L. Afferrante, G. Carbone. Effect of thickness and boundary conditions on the behavior of viscoelastic layers in sliding contact with wavy profiles, *J Mech Phys Solids*, 95 (2016) 517-529.
- [60] N. Menga, L. Afferrante, G.P. Demelio, G. Carbone. Rough contact of sliding viscoelastic layers: numerical calculations and theoretical predictions. *Tribol Int*, 122 (2018) 67-75.
- [61] N. Menga, L. Afferrante, G. Carbone. Adhesive and adhesiveless contact mechanics of elastic layers on slightly wavy rigid substrates. *Int J Solids Struct* 88 (2016) 101-109.
- [62] N. Menga, C. Putignano, L. Afferrante, G. Carbone. The Contact Mechanics of Coated Elastic Solids: Effect of Coating Thickness and Stiffness. *Tribol Let*, 67 (2019) 24.
- [63] N. Menga. Rough frictional contact of elastic thin layers: the effect of geometrical couplig. *Int J Solids Struct*, 164 (2019) 212-220.
- [64] Menga, N., Bottiglionne, F., & Carbone, G. (2019). The indentation rolling resistance in belt conveyors: A model for the viscoelastic friction. *Lubricants*, 7(7), 58.
- [65] B.P. Demidovich, I.A. Maron, *Fundamentals of computational mathematics*. Fizmatgiz, Moscow, 1963.
- [66] Thomson, W. T., & Dahleh, M. D. *Theory of vibration with applications*, Prentice Hall, 1998.
- [67] Irpinia (IT) 1980 90° shock:  $M_w = 6.9$ . ID: IT-1980-0012. Izmit (TR) 1999 90° shock:  $M_w = 7.6$ . ID: TK-1999-0077. Waiiau (NZ) 2016 152° shock:  $M_w = 7.82$ . ID: 20161113\_110256\_WTMC\_20. Kathmandu (NP) 2015 0° shock:  $M_w = 7.8$ . ID: us20002926. Christchurch (NZ) 2010 60° shock:  $M_w = 7.1$ . ID: 20100903\_163541\_GDLC.
- [68] A. Preumont, K. Seto, *Active control of structures*. John Wiley & Sons, 2008.
- [69] C.L. Ng, Y.L. Xu. Semi-active control of a building complex with variable friction dampers. *Eng Struct*, 29 (2007) 1209-1225.
- [70] A. Yanik, U. Aldemir, M. Bakioglu. A new active control performance index for vibration control of three-dimensional structures. *Eng Struct*, 62 (2014) 53-64.
- [71] F. Sadek, B. Mohraz. Semiactive control algorithms for structures with variable dampers. *J Eng Mech*, 124 (1998) 981-990.